Chapter 3
Seismic Performance of Tuned Mass Dampers with Uncertain Parameters

C. Adam, M. Oberguggenberger, and B. Schmelzer

Abstract This chapter addresses the seismic performance of Tuned Mass Dampers (TMDs). In the design of a TMD, two types of uncertainty are relevant: the stochastic excitation modeling the earthquake, and the inherent uncertainty of internal parameters of the damping device and the subsoil. Modeling the excitation by a continuous-time stochastic process the structure-damper system can be described by a linear system of stochastic differential equations. The response is a stochastic process depending on the uncertain parameters of the damping device and the subsoil. These uncertainties are modeled by random sets, i.e., interval-valued random variables. A framework is presented here that admits the combination of these two types of uncertainty leading to a set-valued stochastic process, which is interpreted as containing the true system response. The approach is applied to show how the efficiency of TMDs can be realistically assessed in the presence of uncertainty. The main focus of this paper is on non-stationary models for the excitation based on colored noise multiplied by a prescribed intensity function.

C. Adam (✉)
Unit of Applied Mechanics, University of Innsbruck, Technikerstr. 13, 6020 Innsbruck, Austria
e-mail: christoph.adam@uibk.ac.at

M. Oberguggenberger
Unit of Engineering Mathematics, University of Innsbruck, Technikerstr. 13, 6020 Innsbruck, Austria
e-mail: michael.oberguggenberger@uibk.ac.at

B. Schmelzer
Unit of Engineering Mathematics, University of Innsbruck, Innsbruck, Austria
e-mail: bernhard.schmelzer@uibk.ac.at

G. Hofstetter (ed.), *Computational Engineering*, DOI 10.1007/978-3-319-05933-4_3,

3.1 Introduction

The protection of vibration-prone structures against excessive dynamic response can be accomplished with various passive, active, and semi-active measures, depending on the complexity of the problem, available resources, expected lifespan, available technological standard, environmental conditions, etc. [31, 32]. Since these structures exhibit in general low inherent damping, the installation of a Tuned Mass Damper (TMD) [8] is one effective classical measure to add damping. A TMD is a simple vibratory mechanical device with a single dynamic degree-of-freedom (SDOF) of either mass-spring-dashpot or a pendulum-dashpot type. When appropriately designed, the kinetic energy is transferred from the vibrating structure to the TMD, where it is subsequently dissipated through its viscous element. From the perspective of its weight added to the structure, visual appearance, and space considerations the maximum mass ratio, i.e. the ratio of TMD mass and effective structural mass, is limited in general to 8 %. The efficiency of this device depends on appropriate tuning of its system parameters and on the frequency content of the excitation.

In current engineering practice, TMDs are frequently used to reduce narrow-band structural vibrations induced by wind, traffic, machines, etc. For the tuning of TMD system parameters and prediction of the actual response reduction analytic relations are readily available [8, 14, 40]. However, the efficiency of a TMD to mitigate broad-band earthquake-induced structural vibrations is a topic that is still controversially discussed [5, 13, 17, 26]. Nonetheless, the seismic behavior of a TMD aimed at particularly protecting the building against narrow-band vibrations (excited, e.g., by wind) needs to be assessed reliably if the building is located in an earthquake environment [37]. For example, the stroke, i.e., the peak displacement of the TMD, must not exceed a certain design limit when subjected to severe earthquake excitation with low probability of occurrence [18,39]. Consequently, one objective of this paper is to provide a fundamental study of the seismic performance of a TMD attached to a vibration-prone load-bearing structure that can be modeled as SDOF system.

Seismic assessment of a TMD should consider the quantification of aleatory and epistemic uncertainties. The record-to-record variability of the earthquake excitation is the source of aleatory uncertainty. One option to capture the aleatory uncertainty of the structure-TMD interaction system is to evaluate the responses to several base accelerations with overall characteristic properties recorded during real earthquakes. Based on this approach recent studies [1, 37, 38] have revealed that a TMD reduces the root mean square response effectively, depending on the mass ratio, inherent structural damping, and fundamental structural frequency. However, it was also shown that a TMD might be less avid to decrease the seismic peak response. Additionally, in [37] analytic approximations of the response quantities for design purposes have been derived. Analytic stochastic excitation modeling of earthquake records (see e.g. [25]) is an alternative approach to capture aleatory uncertainty that is more feasible if the earthquake hazard is not well defined.

Epistemic uncertainties result from the lack of knowledge of internal parameters as well as from approximations to reality of the underlying mechanical model. Here the effect of detuned TMD parameters comes into play, which can be traced back to their internal uncertainty. Structural and TMD parameters can only be determined within certain bounds, and they may be subject to change in the course of time. For example, the stiffness of the soil, and as consequence, natural frequencies of the vibration-prone structure depend on environmental conditions such as temperature and moisture.

In this paper, a framework is presented that admits the combination of stochastic processes (i.e., the earthquake excitation) and interval type parameter uncertainty modeled by random sets (i.e., epistemic uncertainty). In particular, modeling the excitation by a continuous-time stochastic process the structure-TMD system is described by a linear system of stochastic differential equations. The system response is a stochastic process depending on the uncertain parameters of the damping device and the subsoil. These uncertainties are modeled by random sets, i.e., finitely many intervals each coming with a probability weight. The approach is applied to show how the efficiency of passive damping mechanisms can be realistically assessed in the presence of uncertainty. In contrast to a previous study [29], where the ground motion was modeled by white noise, in the following colored noise based on the Kanai–Tajimi power spectral density function [15, 34] describes the base acceleration, which is more realistic for earthquake excitation. Preliminary results of the present study have been presented in [28].

3.2 Mechanical Model

This study discusses the vibration mitigation of earthquake excited linear elastic load-bearing structures, whose dynamic response is primarily governed by the fundamental mode. In general, the mechanical model of an SDOF oscillator represents this category of structures with sufficient accuracy. Subsequently, m_s, k_s, and c_s represent lumped mass, stiffness, and viscous damping parameter of this main system. A second SDOF oscillator with lumped mass m_d ($\ll m_\mathrm{s}$), stiffness parameter k_d, and viscous damping parameter c_d serves as TMD. Combined in series this yields the non-classically damped system shown in Fig. 3.1 with two dynamic degrees-of-freedom, expressed by the displacement x_s of the structure and of the TMD x_d, both measured relative to the base displacement x_g. When subjected to base acceleration $\ddot{x}_\mathrm{g}$, the coupled equations of motion of this system read as follows:

$$\mathbf{M}\begin{bmatrix}\ddot{x}_\mathrm{s}\\ \ddot{x}_\mathrm{d}\end{bmatrix}+\mathbf{C}\begin{bmatrix}\dot{x}_\mathrm{s}\\ \dot{x}_\mathrm{d}\end{bmatrix}+\mathbf{K}\begin{bmatrix}x_\mathrm{s}\\ x_\mathrm{d}\end{bmatrix}=\begin{bmatrix}-1\\ -\mu\end{bmatrix}\ddot{x}_\mathrm{g} \tag{3.1}$$

where

$$\mathbf{M}=\begin{bmatrix}1 & 0\\ 0 & \mu\end{bmatrix},\quad \mathbf{C}=\begin{bmatrix}2\zeta_\mathrm{s}\omega_\mathrm{s}+2\zeta_\mathrm{d}\omega_\mathrm{d}\mu & -2\zeta_\mathrm{d}\omega_\mathrm{d}\mu\\ -2\zeta_\mathrm{d}\omega_\mathrm{d}\mu & 2\zeta_\mathrm{d}\omega_\mathrm{d}\mu\end{bmatrix},\quad \mathbf{K}=\begin{bmatrix}\omega_\mathrm{s}^2+\omega_\mathrm{d}^2\mu & -\omega_\mathrm{d}^2\mu\\ -\omega_\mathrm{d}^2\mu & \omega_\mathrm{d}^2\mu\end{bmatrix}$$

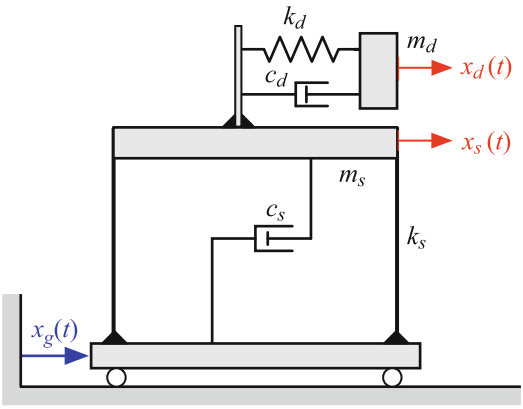

Fig. 3.1 Mechanical model of an SDOF vibration-prone structure equipped with a TMD

The variable μ denotes the mass ratio,

$$\mu = \frac{m_\mathrm{d}}{m_\mathrm{s}}$$

ω_s and ω_d are the natural circular frequencies, and ζ_s and ζ_d denote the non-dimensional damping coefficients of the stand-alone main system and the detuned TMD, respectively,

$$\omega_\mathrm{s} = \sqrt{\frac{k_\mathrm{s}}{m_\mathrm{s}}}, \quad \omega_\mathrm{d} = \sqrt{\frac{k_\mathrm{d}}{m_\mathrm{d}}}, \quad \zeta_\mathrm{s} = \frac{c_\mathrm{s}}{2\omega_\mathrm{s} m_\mathrm{s}}, \quad \zeta_\mathrm{d} = \frac{c_\mathrm{d}}{2\omega_\mathrm{d} m_\mathrm{d}}$$

For an effective reduction of the structural response x_s the parameters of the TMD, i.e., the damping coefficient ζ_d and the frequency ratio δ,

$$\delta = \frac{\omega_\mathrm{d}}{\omega_\mathrm{s}} \tag{3.2}$$

must be tuned "optimally." In general, optimal TMD parameters depend on the type of excitation (harmonic, white noise, etc.) and on the considered response quantity to be optimized (relative or absolute structural displacement or acceleration), see e.g., [3,8,14]. For stationary Gaussian white noise base excitation of an SDOF main system without inherent structural damping (i.e., $\zeta_\mathrm{s} = 0$) the following analytic expressions of optimal TMD parameters have been derived,

$$\delta_\mathrm{opt} = \frac{\sqrt{1-\mu/2}}{1+\mu}, \quad \zeta_\mathrm{d,opt} = \sqrt{\frac{\mu(1-\mu/4)}{4(1+\mu)(1-\mu/2)}} \tag{3.3}$$

assuming that the variance of the stationary relative displacement x_s is minimized, e.g., [3] and [32, p. 234]. Tuning of a TMD according to these expressions minimizes the variance of the relative displacement x_s of the SDOF main system.

3.3 Modeling of the Earthquake Excitation

As outlined in the introduction, base excitation is modeled by a stochastic process. An $\mathbb{R}^d$-valued *stochastic process* $\mathbf{x}$ on a time interval $[0, \bar{t}]$ assigns to each point of time t a random variable $\mathbf{x}(t)$, defined on a probability space Ω with its σ-algebra Σ of measurable sets and the probability measure P. The process is specified if the finite dimensional joint distributions of all random variables $\mathbf{x}(t)$, $t \in [0, \bar{t}]$ are known. A one-dimensional Brownian motion (Wiener process) b is defined for $t \in [0, \infty)$ as follows: each $b(t)$ is a Gaussian variable with mean zero and variance t. Further, the covariance of $b(t_1)$ and $b(t_2)$ equals $\min(t_1, t_2)$ and $b(0) = 0$. The corresponding probability space is denoted by $(\Omega_b, \Sigma_b, P_b)$. Here and in the sequel variable ν_b is reserved for the elements of the space Ω_b with a similar convention for the other probability spaces.

Continuous time white noise $\dot{b}$ is the weak derivative of Brownian motion. It is a generalized process with mean zero, infinite variance, and zero covariance. It is formalized here by means of Itô's integral, for which the reader is referred to the literature, e.g., [2, 22].

Systems of ordinary differential equations with white noise excitation are handled as Itô stochastic differential equations (SDEs):

$$\mathrm{d}\mathbf{x}(t) = \mathbf{f}\big(t, \mathbf{x}(t)\big)\,\mathrm{d}t + \mathbf{g}\big(t, \mathbf{x}(t)\big)\,\mathrm{d}b(t)$$

interpreted as the integral equation

$$\mathbf{x}(t) = \mathbf{x}_0 + \int_0^t \mathbf{f}\big(s, \mathbf{x}(s)\big)\,\mathrm{d}s + \int_0^t \mathbf{g}\big(s, \mathbf{x}(s)\big)\,\mathrm{d}b(s)$$

where time t ranges in some finite time interval $[0, \bar{t}]$, $\mathbf{x}_0$ is a random variable representing the initial value, $\mathbf{f}, \mathbf{g} : [0, \bar{t}] \times \mathbb{R}^d \to \mathbb{R}^d$ are coefficient functions, and b is a one-dimensional Wiener process on $(\Omega_b, \Sigma_b, P_b)$. Their solutions are stochastic processes with continuous trajectories.

In [29] the authors have used white noise to model the base acceleration, for the sake of simplicity. White noise is—due to its covariance structure—a stationary process with a constant power spectral density. Hence, all frequencies appear equally in the base acceleration, which is a contradiction to the properties of most recorded ground motions. Furthermore, the infinite variance can actually not be interpreted physically. Thus, the main goal of the present paper is to use a more realistic model for ground acceleration.

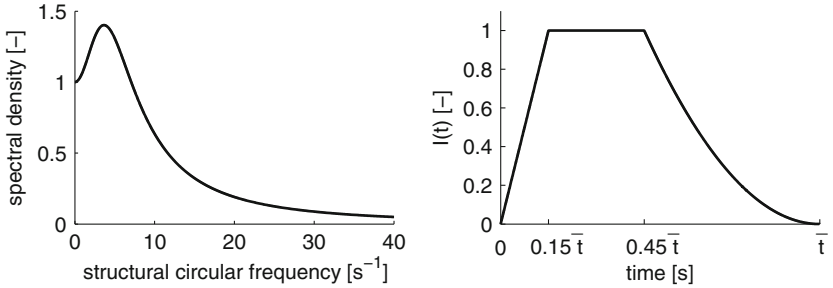

Fig. 3.2 *Left subplot*: power spectral density for Kanai–Tajimi model, $\omega_g = 5\,\mathrm{rad/s}$, $\zeta_g = 0.9$, $S_0 = 1$; *right subplot*: intensity function

In the literature (see, e.g., [4, 24, 33]) one can often find a model proposed by Kanai and Tajimi [15,34]. In their approach the base acceleration of the earth surface layer is approximated by the absolute acceleration of a linear SDOF oscillator excited by white noise. The corresponding equation of motion reads as follows

$$\ddot{z}(t) + 2\zeta_g\omega_g\dot{z}(t) + \omega_g^2 z(t) = -\dot{b}(t)$$

where ω_g and ζ_g are, respectively, the natural circular frequency and non-dimensional damping coefficient of the oscillator corresponding to the properties of the subsoil. The above equation can be written as a two-dimensional linear system of stochastic differential equations,

$$\mathrm{d}\mathbf{z}(t) = \begin{bmatrix} 0 & 1 \\ -\omega_g^2 & -2\zeta_g\omega_g \end{bmatrix} \mathbf{z}(t)\,\mathrm{d}t + \begin{bmatrix} 0 \\ -1 \end{bmatrix} \mathrm{d}b(t)$$

where $\mathbf{z} = [z, \dot{z}]^\mathsf{T}$. The ground acceleration is then modeled by the absolute acceleration of the oscillator, that is $\ddot{x}_g = \ddot{z} + \dot{b}$, which results in the following stochastic process

$$\ddot{x}_g(t) = -2\zeta_g\omega_g\dot{z}(t) - \omega_g^2 z(t) \tag{3.4}$$

Its power spectral density is given by the equation

$$S(\omega) = S_0\,\frac{\omega_g^4 + 4\zeta_g^2\omega_g^2\omega^2}{(\omega_g^2 - \omega^2)^2 + 4\zeta_g^2\omega_g^2\omega^2} \tag{3.5}$$

where S_0 is the (constant) power spectral density of white noise. Obviously, the spectral density S is not constant and thus represents a special type of colored noise. The left picture in Fig. 3.2 shows a plot of the power spectral density for the soil parameters $\omega_g = 5\,\mathrm{rad/s}$, $\zeta_g = 0.9$, and for the uniform spectral density $S_0 = 1$.

Note that the process given by Eq. (3.4) is (asymptotically) stationary. However, it is a well-known fact that the base acceleration of earthquakes is non-stationary.

Typically, at the beginning of the earthquake, amplitudes of the base acceleration are increasing. After a period of quasi-stationary strong motion, amplitudes are decreasing again. Thus, it seems reasonable to multiply the process from Eq. (3.4) with some intensity function I corresponding to the non-stationary behavior of the base acceleration (see, e.g., [6]). This leads to the following model for $\ddot{x}_g$:

$$\ddot{x}_g(t) = I(t)\big(-2\zeta_g\omega_g\dot{z}(t) - \omega_g^2 z(t)\big) \tag{3.6}$$

As suggested in [24] the intensity function plotted in the right-hand side picture of Fig. 3.2 is used: During the first 15 % of the total duration of the earthquake, I increases linearly from 0 to 1. After a constant period over 30 % of the earthquake duration, I decreases in a quadratic manner.

Rewriting the coupled equations of motion from (3.1) as a system of first order, and introducing the stochastic process (3.6) for the base acceleration leads to the following six-dimensional linear system of stochastic differential equations:

$$\mathrm{d}\mathbf{x}(t) = \mathbf{F}(t)\mathbf{x}(t)\,\mathrm{d}t + \mathbf{g}\,\mathrm{d}b(t) \tag{3.7}$$

where $\mathbf{x} = [x_s, x_d, z, \dot{x}_s, \dot{x}_d, \dot{z}]^\mathsf{T}$, $\mathbf{g} = [0,0,0,0,0,-1]^\mathsf{T}$ and

$$\mathbf{F}(t) = \begin{bmatrix} 0 & 0 & 0 & 1 & 0 & 0 \\ 0 & 0 & 0 & 0 & 1 & 0 \\ 0 & 0 & 0 & 0 & 0 & 1 \\ -\omega_s^2 - \omega_d^2\mu & \omega_d^2\mu & -\omega_g^2 I(t) & -2\zeta_s\omega_s - 2\zeta_d\omega_d\mu & 2\zeta_d\omega_d\mu & -2\zeta_g\omega_g I(t) \\ \omega_d^2 & -\omega_d^2 & -\omega_g^2 I(t) & 2\zeta_d\omega_d & -2\zeta_d\omega_d & -2\zeta_g\omega_g I(t) \\ 0 & 0 & -\omega_g^2 & 0 & 0 & -2\zeta_g\omega_g \end{bmatrix}$$

Note that all parameters of the model are contained in the system matrix $\mathbf{F}$. Furthermore, $\mathbf{F}$ is time-dependent because of the intensity function I. This contrasts the situation considered in [29], where the system matrix does not depend on time.

For reasons of comparison, the response of the system without TMD is considered, too. In this case the motion of the corresponding SDOF oscillator is described by the equation

$$\ddot{\tilde{x}}_s + 2\zeta_s\omega_s\dot{\tilde{x}}_s + \omega_s^2\tilde{x}_s = -\ddot{x}_g$$

Substituting the stochastic process (3.6) for $\ddot{x}_g$ leads to the first order SDE system

$$\mathrm{d}\tilde{\mathbf{x}}(t) = \begin{bmatrix} 0 & 0 & 1 & 0 \\ 0 & 0 & 1 & 0 \\ -\omega_s^2 & -\omega_g^2 & -2\zeta_s\omega_s & -2\zeta_g\omega_g \\ 0 & -\omega_g^2 & 0 & -2\zeta_g\omega_g \end{bmatrix} \tilde{\mathbf{x}}(t)\,\mathrm{d}t + \begin{bmatrix} 0 \\ 0 \\ 0 \\ -1 \end{bmatrix} \mathrm{d}b(t) \tag{3.8}$$

where $\tilde{\mathbf{x}} = [x_s, z, \dot{x}_s, \dot{z}]^T$. In both systems (3.7) and (3.8) the initial values are assumed to be zero.

3.4 Modeling of the Parameter Uncertainty

The epistemic parameter uncertainty is accounted for by means of random sets. In general, a *random set* is a set-valued random variable satisfying certain measurability conditions. The simplest case arises when the underlying probability space is finite. In this case, one speaks of *finite random sets* or *Dempster–Shafer structures*. Such a structure is given by finitely many subsets $A_i, i = 1, \ldots, n$ of a given set $\mathbb{A}$, called the *focal elements*, each of which comes with a *probability weight* p_i, $\sum p_i = 1$.

For example, each set A_i could be the result of an interval-valued measurement and p_i its relative frequency in a sample. Alternatively, the sets A_i could be ranges of a variable obtained from source number i with relative credibility p_i.

As a random set, a Dempster–Shafer structure is viewed as given by an n-point probability space $\Omega_{\mathbb{A}} = \{1, 2, \ldots, n\}$ with probability masses $\{p_1, p_2, \ldots, p_n\}$. The assignment $i \to A_i$ is the defining set-valued random variable.

Following Dempster and Shafer [7, 30], two important set functions are introduced: the *lower probability* and the *upper probability* of an event B are defined by

$$\underline{P}(B) = \sum_{A_i \subset B} p_i, \qquad \overline{P}(B) = \sum_{A_i \cap B \neq \emptyset} p_i \tag{3.9}$$

A good visualization of a random set can be given through its *contour function* on the basic space $\mathbb{A}$, assigning each singleton a its upper probability:

$$a \to \overline{P}(\{a\}) \tag{3.10}$$

It is simply obtained by adding the probability weights p_i of those focal elements A_i to which a belongs. Figure 3.3 shows a random set and the resulting contour function where weights have been chosen as $p_1 = 1/2$, $p_2 = 1/3$, $p_3 = 1/6$.

In the sequel, random sets are needed that are defined on an arbitrary probability space $(\Omega_{\mathbb{A}}, \Sigma_{\mathbb{A}}, P_{\mathbb{A}})$ and whose values are subsets of p-dimensional coordinate space $\mathbb{A} = \mathbb{R}^p$. More precisely, random compact intervals are used, that is, random variables

$$A : \Omega_{\mathbb{A}} \to \mathscr{I}_c(\mathbb{A})$$

where $\mathscr{I}_c(\mathbb{A})$ denotes the set of all non-empty compact intervals in $\mathbb{A}$. Random compact intervals are used since they have and imply advantageous theoretical

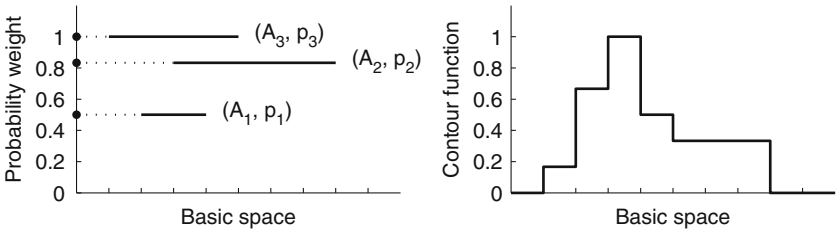

Fig. 3.3 A random set and its contour function; the *three dots* on the vertical axis symbolize the underlying three-point probability space

properties (e.g., concerning measurability, see [19]). In analogy to (3.9) the lower probability and the upper probability of an event B are defined as

$$\underline{P}(B)=P_{\mathbb{A}}(\{\nu_{\mathbb{A}} \in \Omega_{\mathbb{A}} : A(\nu_{\mathbb{A}}) \subseteq B\}), \quad \overline{P}(B)=P_{\mathbb{A}}(\{\nu_{\mathbb{A}} \in \Omega_{\mathbb{A}} : A(\nu_{\mathbb{A}}) \cap B \neq \emptyset\}) \tag{3.11}$$

The event B may be taken as any Borel measurable subset of $\mathbb{A}$. The contour function is given by (3.10).

For further details on interpretations and applications the reader is referred to the articles [10–12, 21, 35, 36] as well as to the monographs [19, 20].

3.4.1 Two Examples of Random Sets for Uncertainty Modeling

In [29] random sets constructed from Tchebycheff's inequality have been used, which require only minimal information about the parameters. More precisely, let a be an uncertain parameter preliminarily viewed as a random variable with expectation (or nominal) value $\overline{a}$ and variance σ^2. Then one can define a random set A on $\Omega_{\mathbb{A}} = (0, 1]$ by setting

$$A(\nu) = \left[\overline{a} - \tfrac{\sigma}{\sqrt{\nu}}, \overline{a} + \tfrac{\sigma}{\sqrt{\nu}}\right], \quad \nu \in \Omega_{\mathbb{A}} \tag{3.12}$$

where $\Omega_{\mathbb{A}} = (0, 1]$ is equipped with the uniform probability distribution. It has been argued in [29] that a focal element $A(\nu)$ may be viewed as an approximate two-sided $(1-\nu)$-fractile range for the parameter a. Furthermore, it has been explained how to compute σ from a probabilistic estimate about the range of the parameter. Figure 3.4 shows the contour function of a generic Tchebycheff random set.

In view of the shape of its contour function, it is obvious that a Tchebycheff random set is an appropriate model for parameter uncertainty when a parameter can take arbitrary (real) values, and negative deviations from the expectation or nominal value seem as likely as positive deviations. In case the parameter range is strictly bounded on (only) one side of the nominal value, it might be better to choose a random set whose contour function reflects this asymmetry.

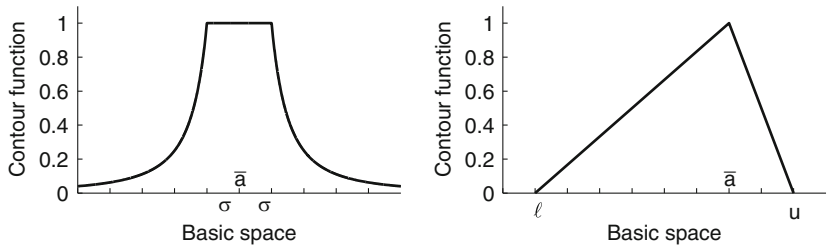

Fig. 3.4 *Left subplot*: a generic Tchebycheff random set; *right subplot*: a triangular random set

One possibility is to use a random set whose contour function has a triangular shape. The latter is then determined by a nominal value $\overline{a}$ and the lower and upper bounds ℓ, u of the parameter range. Such a random set can be defined on $\Omega_{\mathbb{A}} = [0, 1]$ by setting

$$A(\nu) = \big[\ell + (\overline{a} - \ell)\nu, u - (u - \overline{a})\nu\big], \quad \nu \in [0, 1]$$

where $\Omega_{\mathbb{A}} = [0, 1]$ is equipped with the uniform probability distribution. The right picture in Fig. 3.4 shows the contour function of a triangular random set.

3.5 Combination of Stochastic Excitation and Parameter Uncertainty

In the previous two sections it has been demonstrated how to model the base acceleration by stochastic processes and how to use random sets to model (epistemic) parameter uncertainty. The purpose of this section is to demonstrate how the two types of uncertainty can be combined to obtain set-valued assessments of the TMD performance.

As it has been shown at the end of Sect. 3.3, the motion of the combined structure-damper system is described by the linear system of SDEs (3.7), where the parameters μ, ζ_{s}, ω_{s}, ζ_{d}, ω_{d}, ζ_{g}, ω_{g} appear in the system matrix $\mathbf{F}$. In Sect. 3.6, various of these parameters are assumed to be uncertain, and random intervals presented in Sect. 3.4 are used. Note that this is in contrast to [29], where only TMD parameters were assumed to be uncertain. Corresponding to the situation, the tuple of uncertain parameters is denoted by a. The linear system (3.7) then reads

$$\mathrm{d}\mathbf{x}_a(t) = \mathbf{F}(t, a)\mathbf{x}_a(t)\,\mathrm{d}t + \mathbf{g}\,\mathrm{d}b(t)$$

where $\{\mathbf{x}_a(t)\}_{t\in[0,\bar{t}]}$ denotes the solution process corresponding to parameter value a.

As a first indicator for the performance of the TMD the displacement x_{s} of the structure is considered. More precisely, x_{s} is scaled by the largest structural displacement $\tilde{x}_{\mathrm{s}}$ when no TMD is attached. This leads to a map y defined on the

time interval, the set of possible parameter values $\mathbb{A}$, and the probability space Ω_b of Brownian motion:

$$y_a(t, \nu_b) = \frac{x_{s,a}(t, \nu_b)}{\max_{t\in[0,\bar{t}]} |\tilde{x}_{s,a}(t, \nu_b)|}$$

The latter can be seen as a non-dimensional displacement.

The aim is now to combine both kinds of uncertainty. To this end, the set-valued function

$$Y(t, \nu) = \{y_a(t, \nu_b) : a \in A(\nu_{\mathbb{A}})\} \tag{3.13}$$

is introduced, where $(t, \nu) \in [0, \bar{t}] \times \Omega$ and (Ω, Σ, P) denotes the product probability space

$$(\Omega, \Sigma, P) = (\Omega_{\mathbb{A}} \times \Omega_b, \Sigma_{\mathbb{A}} \otimes \Sigma_b, P_{\mathbb{A}} \otimes P_b)$$

This definition means that for each time t and each element $\nu = (\nu_{\mathbb{A}}, \nu_b)$ of the product space Ω the corresponding values of the non-dimensional displacement are merged to one set $Y(t, \nu)$, which is interpreted as containing the true value of the structural non-dimensional displacement. Note that Y is a set-valued stochastic process, that is, at each time t one has a random set $Y(t)$, whose values are compact intervals in $\mathbb{R}$. For further details the reader is referred to [27], where the theory of this approach has been developed.

For reasons of comparison the non-dimensional displacement $\tilde{y}$ of the structure without TMD

$$\tilde{y}_a(t, \nu_b) = \frac{\tilde{x}_{s,a}(t, \nu_b)}{\max_{t\in[0,\bar{t}]} |\tilde{x}_{s,a}(t, \nu_b)|}$$

is also considered. If parameters of the base acceleration are assumed to be uncertain, a set-valued process $\tilde{Y}$ can be defined from the processes $\tilde{y}_a$ in a similar manner as in Eq. (3.13). Furthermore, the absolute values of the non-dimensional displacements y_a are of interest, too, resulting in the set-valued process

$$|Y|(t, \nu) = \{|y_a(t, \nu_b)| : a \in A(\nu_{\mathbb{A}})\}$$

The reader is referred to [29] for equations of the boundary processes of $|\tilde{Y}|$ and their mean value functions.

A central concern is the effectiveness of the TMD, that is, to which extent the dynamic response x_s is reduced compared to the response $\tilde{x}_s$ when no TMD is attached. In the single-valued case the peak response reduction coefficient and the root mean square (RMS) response reduction coefficient are considered

$$r_{\mathrm{m},a}(\nu_b) = \frac{\max_{t\in[0,\bar{t}]} |x_{\mathrm{s},a}(t,\nu_b)|}{\max_{t\in[0,\bar{t}]} |\tilde{x}_{\mathrm{s},a}(t,\nu_b)|}, \quad r_{\mathrm{q},a}(\nu_b) = \sqrt{\frac{\int_0^{\bar{t}} x_{\mathrm{s},a}(t,\nu_b)^2\,\mathrm{d}t}{\int_0^{\bar{t}} \tilde{x}_{\mathrm{s},a}(t,\nu_b)^2\,\mathrm{d}t}}$$

For each parameter value a and for each path of the Brownian motion, the map $r_{\mathrm{m},a}$ represents the reduction of the peak displacement of the structure, whereas $r_{\mathrm{q},a}$ computes the quadratic-mean reduction (over time) of $x_{\mathrm{s},a}$. Similar as in Eq. (3.13) these maps can be extended to the set-valued reduction coefficients R_{m} and R_{q} defined by

$$R_{\mathrm{m}}(\nu) = \{r_{\mathrm{m},a}(\nu_b) : a \in A(\nu_{\mathbb{A}})\}, \quad R_{\mathrm{q}}(\nu) = \{r_{\mathrm{q},a}(\nu_b) : a \in A(\nu_{\mathbb{A}})\}$$

whose values are compact subintervals of the unit interval $[0, 1]$.

The stroke of the TMD is an important design parameter to assure the efficiency of the TMD, and to avoid damage of the TMD and/or of the main structure. It represents the TMD peak displacement with respect to its attachment point at the main structure. As with the reduction coefficients $r_{\mathrm{m},a}$ and $r_{\mathrm{q},a}$ the displacement $\tilde{x}_s$ of the structure without TMD is used for normalization. Thus, the equation for the stroke coefficient reads as follows [37]

$$d_a(\nu_b) = \frac{\max_{t\in[0,\bar{t}]} |x_{\mathrm{s},a}(t,\nu_b) - x_{\mathrm{d},a}(t,\nu_b)|}{\max_{t\in[0,\bar{t}]} |\tilde{x}_{\mathrm{s},a}(t,\nu_b)|}$$

Similar as in Eq. (3.13) one can define the set-valued stroke coefficient D by

$$D(\nu) = \{d_a(\nu_b) : a \in A(\nu_{\mathbb{A}})\}$$

whose values are compact intervals.

3.6 Numerical Simulation and Results

Subsequently, results of numerical simulations are presented. Unless otherwise stated, the results are based on the following nominal values: mass ratio $\mu = 0.05$, structural inherent damping $\zeta_{\mathrm{s}} = 0.005$, soil frequency $\omega_{\mathrm{g}} = 5\,\mathrm{rad/s}$ (soil period $T_{\mathrm{g}} \approx 1.26\,\mathrm{s}$), soil damping $\zeta_{\mathrm{g}} = 0.9$. The latter soil values correspond to soil class C according to Eurocode 8, see [9] and [23]. For the nominal values of the TMD parameters ω_{d} and ζ_{d} the optimal values given by Eqs. (3.2) and (3.3) are used.

For each tuple of parameter values approximations are computed using the Order 2 Implicit Strong Taylor Scheme (see [16]). Each simulation involves 500 sample functions of Brownian motion, and (constant) step size Δt of the time discretization is chosen as $\min(T_{\mathrm{s}}, T_{\mathrm{g}})/12$ if $\min(T_{\mathrm{s}}, T_{\mathrm{g}}) < 1$, or $1/20$ otherwise.

3.6.1 Parametric Studies

In this section the results of parametric studies are presented in an effort to reveal how the expectation values of the reduction coefficients and the stroke coefficient are influenced by structural and soil parameters μ, T_s, ζ_s, T_g, and ζ_g, respectively. In each study the structural period $T_s = 2\pi/\omega_s$ is varied in the range from 0.05 to 5 s. Additionally, one of the remaining parameters is varied while the other parameters are fixed to their nominal values. For each output variable a line plot (with the structural period T_s on the abscissa and one of the response quantities r_m, r_q, d on the ordinate) and a contour plot are presented.[1] All results are compared to the outcomes based on white noise base excitation.

Figure 3.5 shows the expected values of the peak and RMS displacement reduction coefficients r_m and r_q and the stroke coefficient d, respectively, for T_s and T_g varying in the range from 0.05 to 5 s. The bold black lines in the left pictures represent the results for white noise base acceleration (further investigated in [29]), whereas the thin (and partially marked) lines correspond to colored noise excitation for various values of the soil period T_g while fixing the soil damping ζ_g to the value 0.9.

Obviously, reduction coefficients r_m and r_q increase with increasing T_g particularly for short period structures, which means that the TMD is less effective for longer soil periods. However, the stroke coefficient is almost not affected by variation of T_g. The results of this figure suggest that for small structural periods T_s the TMD performance for colored noise excitation is worse than for white noise excitation. This behavior is coherent with computations accomplished with real earthquake records (see [37, 38]) and is due to the fact that the power spectral density (3.5) yields small values for high frequencies (small periods), whereas in the white noise case all frequencies equally likely appear. Another observation is that the smaller the soil period T_g the better the reduction plot approaches the white noise curve. For $T_g = 0.05$ s the expectations of the reduction coefficients actually coincide with those of the white noise case. Again, this can be explained by considering the spectral density of the colored noise process: If $\omega_g \to \infty$ (or equivalently $T_g \to 0$) then $S(\omega) \to S_0$ for all ω, that is, S converges to a constant spectral density, and this corresponds to white noise.

Figure 3.6 depicts the reduction and stroke coefficients for nominal soil frequency $\omega_g = 5$ rad/s ($T_g \approx 1.26$ s) and varying soil damping ζ_g ranging from 0.3 to 0.95. It is remarkable that for a structural period of approximately 1.12 s all values of ζ_g lead to the same reduction. In the structural period range larger than this period the considered response quantities remain almost unaffected by the variation of soil damping. However, in the lower period range RMS and peak reduction coefficients increase considerably with decreasing soil damping, i.e., the TMD becomes less effective.

[1] In the sequel, we shall denote the reduction and stroke coefficients simply by r_m, r_q, d in place of $r_{m,a}$, $r_{q,a}$, d_a, unless explicit reference to a specific tuple of parameters a is required.

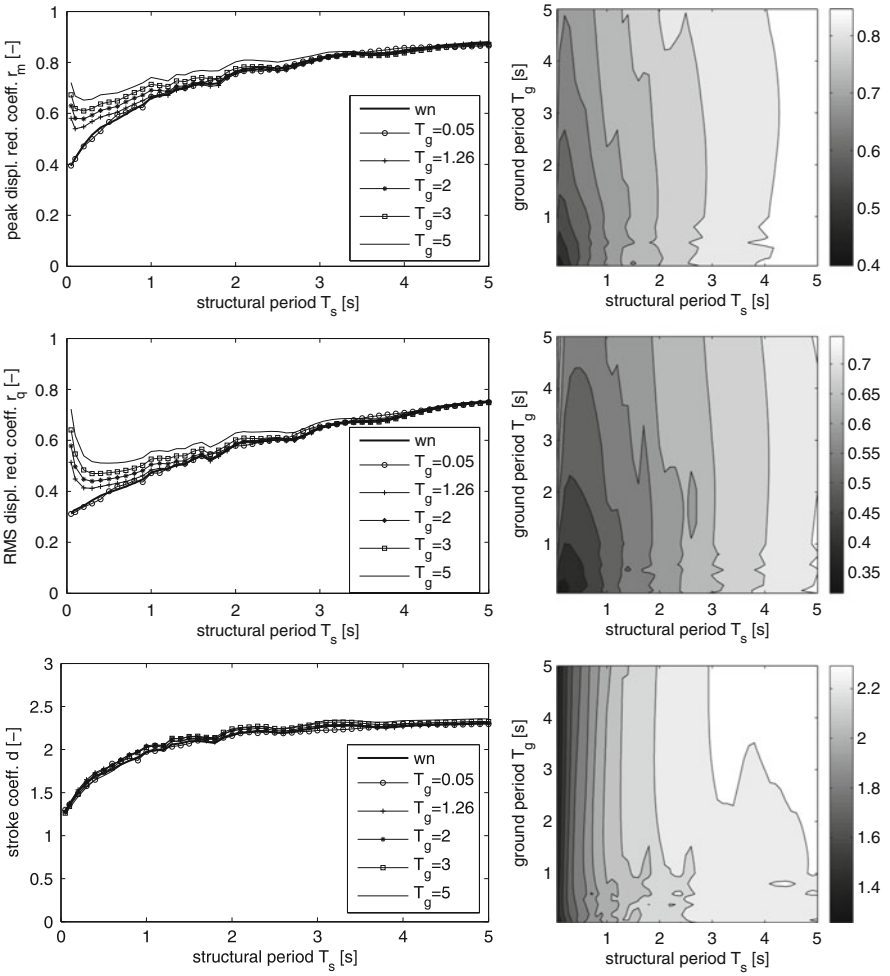

Fig. 3.5 Expectations of reduction coefficients r_{m}, r_{q} and stroke coefficient d, based on white noise excitation (wn) and colored noise excitation for $\zeta_{\mathrm{g}} = 0.9$ and various values of T_{g} [in (s)]

Figure 3.7 shows the behavior of the output variables r_{m}, r_{q}, and d under variation of mass ratio μ in the range of 0.5–8 % based on colored noise excitation with nominal soil parameters ($\omega_{\mathrm{g}} = 5\,\mathrm{rad/s}$, $\zeta_{\mathrm{g}} = 0.9$). One can see that all three output variables decrease when μ increases. This confirms the well-known fact that for larger mass ratios structural displacement is reduced more efficiently and the stroke coefficient is smaller. It is remarkable that for small mass ratios (0.5 % and 1 %) the stroke coefficient depends on the structural period in a non-monotonic manner. From Fig. 3.8 one can conclude that in the case of white noise excitation results are very similar to those based on colored noise excitation, except

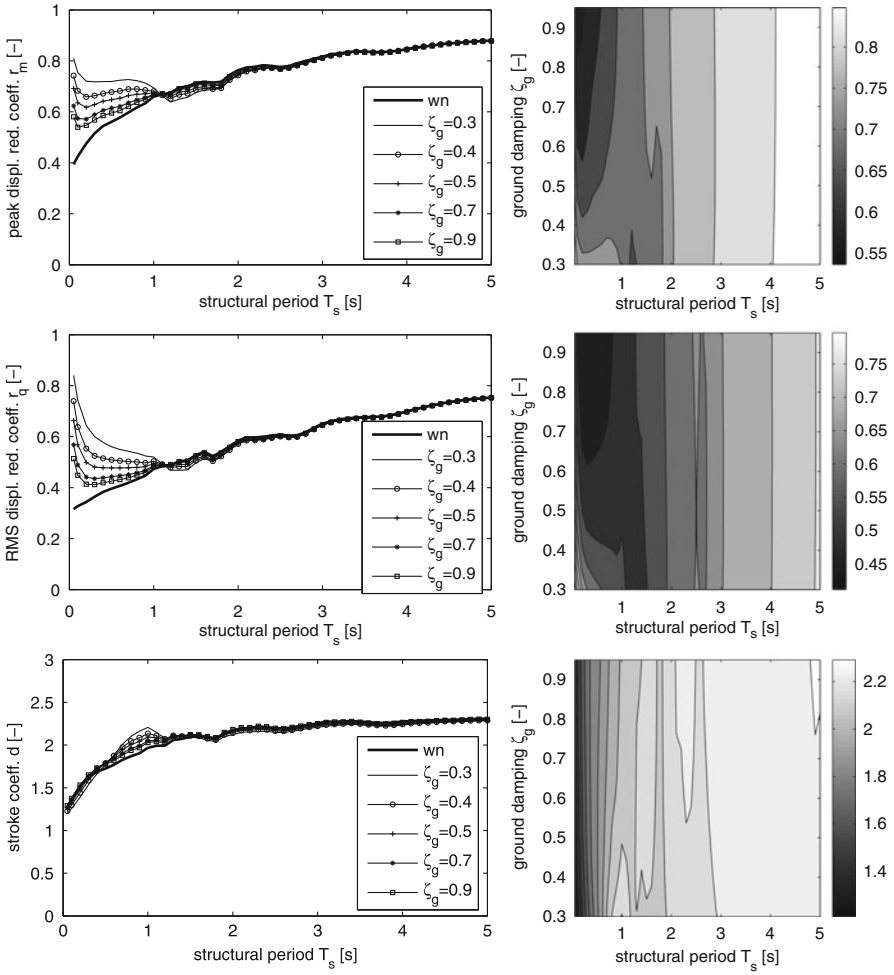

Fig. 3.6 Expectations of reduction coefficients r_m, r_q and stroke coefficient d, respectively, based on white noise excitation and colored noise excitation for $\omega_\mathrm{g} = 5\,\mathrm{rad/s}$ ($T_\mathrm{g} \approx 1.26\,\mathrm{s}$) and various values of ζ_g

for small structural periods, which is coherent with the results displayed in Figs. 3.5 and 3.6. Comparing the results of Figs. 3.7 and 3.8 with outcomes of a study [37] based on a set of recorded ground motions, reveals that not only the dependency of the considered response variables on various structural parameters is the same for the stochastic soil model used here and for real ground motions. These response quantities are even of the same order of magnitude. The approach of this study is thus confirmed.

In Fig. 3.9 results for r_m, r_q, and d are plotted when the structural damping coefficient ζ_s is varied in the range of 0.5–5 %, mass ratio $\mu = 5\,\%$, and the

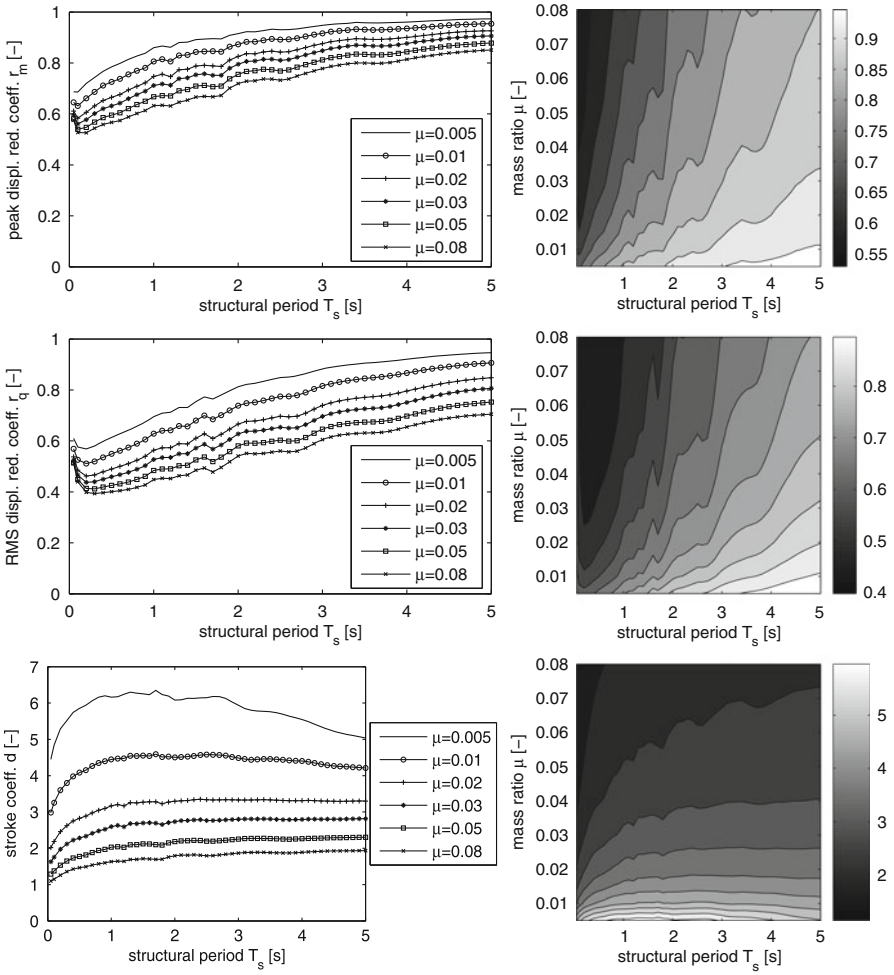

Fig. 3.7 Expectations of reduction coefficients r_{m}, r_{q} and stroke coefficient d based on colored noise excitation ($\omega_{\mathrm{g}} = 5\,\mathrm{rad/s}$, $\zeta_{\mathrm{g}} = 0.9$) for $\zeta_{\mathrm{s}} = 0.005$ and various values of μ, respectively

Kanai–Tajimi model with nominal soil parameters ($\omega_{\mathrm{g}} = 5\,\mathrm{rad/s}$, $\zeta_{\mathrm{g}} = 0.9$) is used. It is readily observed that all three output variables increase when ζ_{s} increases. This means that higher inherent structural damping leads to lower effectiveness of the TMD to reduce the response and to a larger stroke relative to the peak displacement of the main system. This outcome is obvious because the main system becomes less-vibration prone the larger the inherent damping is. From Fig. 3.10 one can see once more that in the case of white noise excitation results are very similar to those based on colored noise excitation, except for small structural periods.

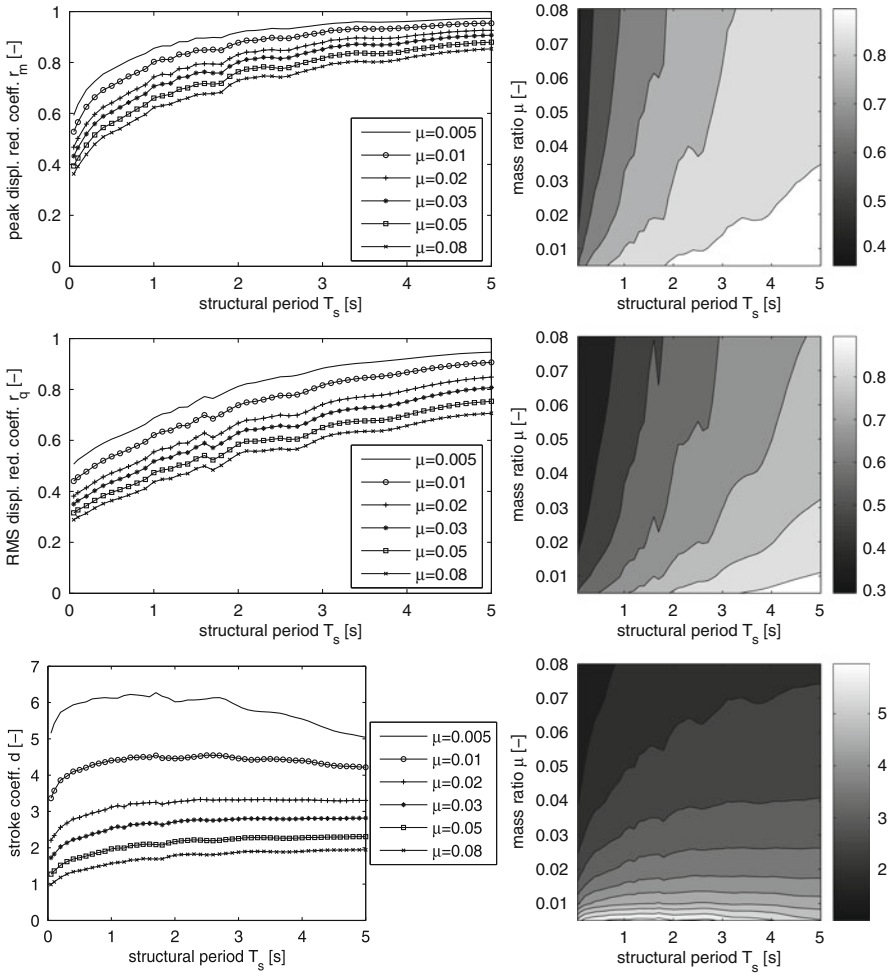

Fig. 3.8 Expectations of reduction coefficients r_{m}, r_{q} and stroke coefficient d, respectively, based on white noise excitation for $\zeta_{\mathrm{s}} = 0.005$ and various values of μ

3.6.2 Set-Valued TMD Parameters

In this subsection the mass ratio μ, the structural inherent damping ζ_{s}, and the soil parameters ω_{g} and ζ_{g} are fixed to their nominal values whereas the TMD parameters ω_{d} and ζ_{d} are assumed to be uncertain. In a first simulation, a Tchebycheff random set A is used only for ω_{d}, and ζ_{d} is assumed to take its nominal value. Concerning the variability it is assumed that the actual value of ω_{d} lies in a range of $\pm 40\,\%$ of its nominal value with 99 % certainty. As explained in [29] this leads to a coefficient of variation of 0.04, that is, $\sigma = 0.04\overline{\omega}_{\mathrm{d}}$. Corresponding to Eq. (3.12) the focal

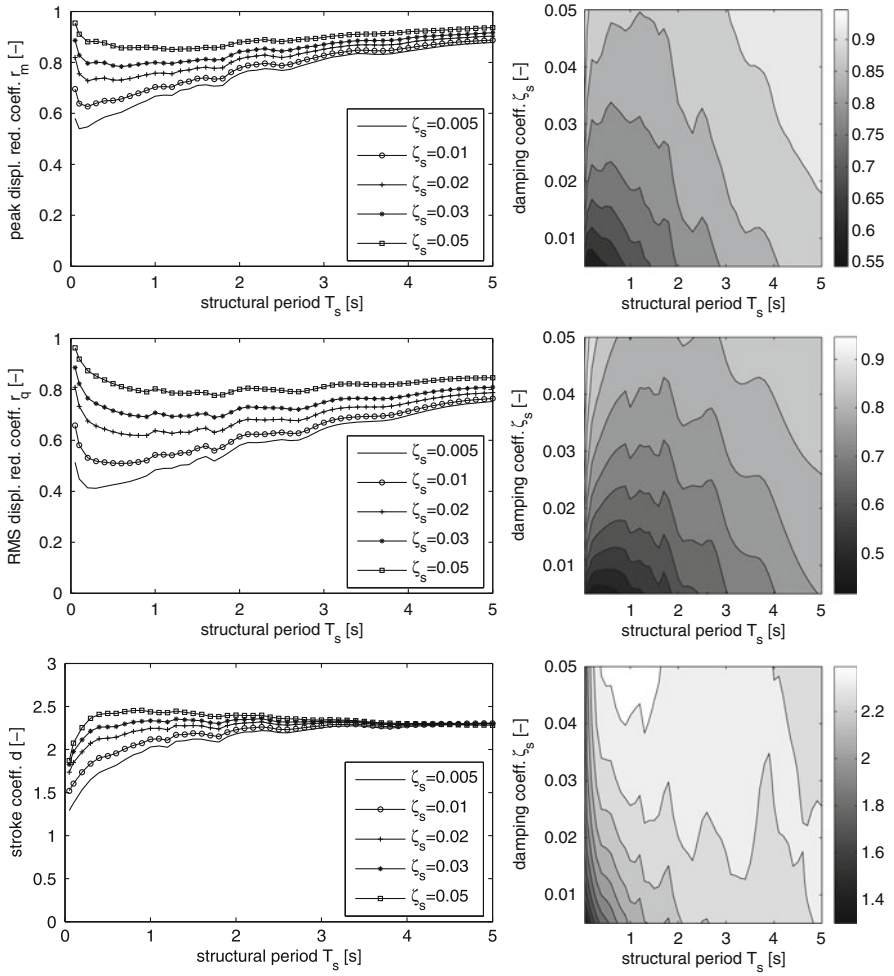

Fig. 3.9 Expectations of reduction coefficients r_m, r_q and stroke coefficient d, respectively, based on colored noise excitation ($\omega_\mathrm{g} = 5\,\mathrm{rad/s}$, $\zeta_\mathrm{g} = 0.9$) for $\mu = 0.05$ and various values of ζ_s

elements are obtained as

$$A(\nu_\mathbb{A}) = \Big[\overline{\omega}_\mathrm{d}\Big(1 - \frac{0.04}{\sqrt{\nu_\mathbb{A}}}\Big), \overline{\omega}_\mathrm{d}\Big(1 + \frac{0.04}{\sqrt{\nu_\mathrm{A}}}\Big)\Big]$$

where $\nu_\mathbb{A} \in (0, 1]$. For the numerical simulation the random set is approximated by a finite random set consisting of the ten focal elements obtained for $\nu_{\mathbb{A},j} = (j/10)^2$, $j = 1, \ldots, 10$. The corresponding weights are then given by $p_1 = 0.01$, $p_j = \nu_{\mathbb{A},j} - \nu_{\mathbb{A},j-1} = (2j-1)/100$, $j = 2, \ldots, 10$. This leads to a better approximation (with respect to the upper and lower probability) than choosing $\nu_{\mathbb{A},j}$ equidistantly from $(0, 1]$.

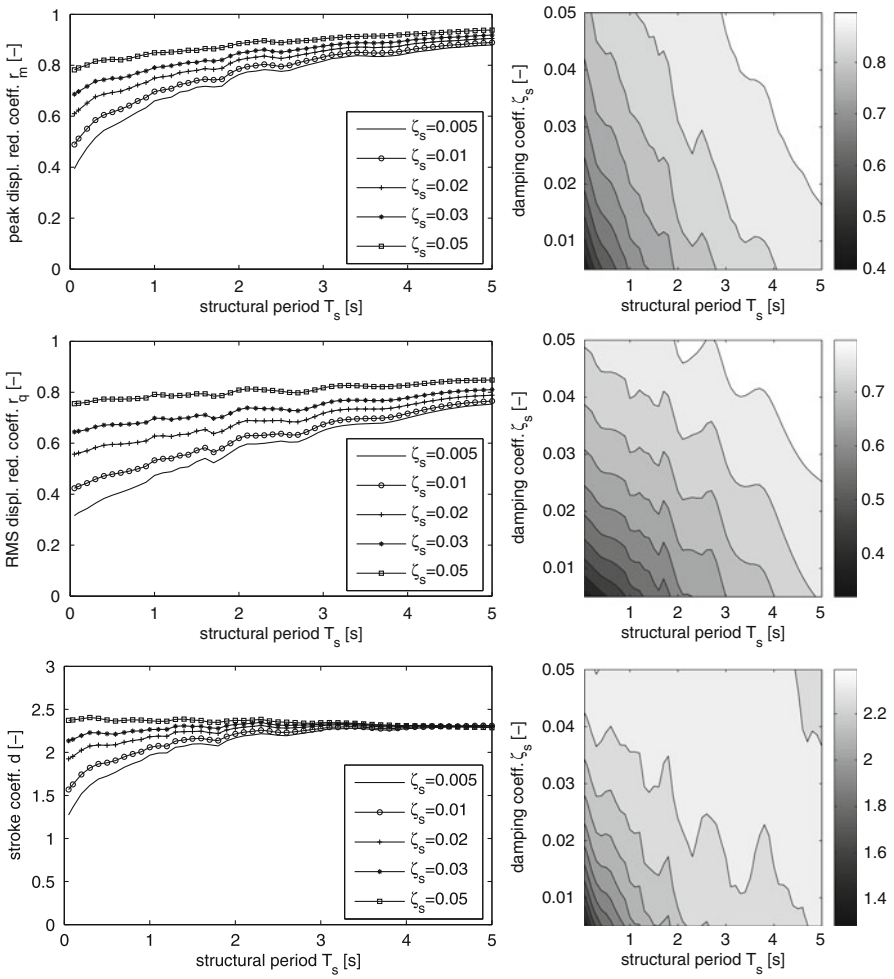

Fig. 3.10 Expectations of reduction coefficients r_{m}, r_{q} and stroke coefficient d, respectively, based on white noise excitation for $\mu = 0.05$ and various values of ζ_{s}

Figure 3.11 shows the expectation of the peak and RMS displacement reduction coefficients and the expectation of the stroke coefficient for 11 different values of the structural period T_{s}, namely, 0.05, 0.5, 1, 1.5, 2, 2.5, 3, 3.5, 4, 4.5, 5 (values in seconds). The outer (bold) lines in the pictures are the interval bounds of the expectation of the set-valued reduction coefficients R_{m}, R_{q} and the set-valued stroke coefficient D, respectively. The central (marked) lines represent the output obtained for the optimal parameter value $\overline{\omega}_{\mathrm{d}}$.

Figure 3.12 is obtained by using a Tchebycheff random set for the TMD damping coefficient ζ_{d} with coefficient of variation of 0.04 and fixing ω_{d} to its optimal value. It seems that varying ζ_{d} has almost no influence on the reduction coefficients, which

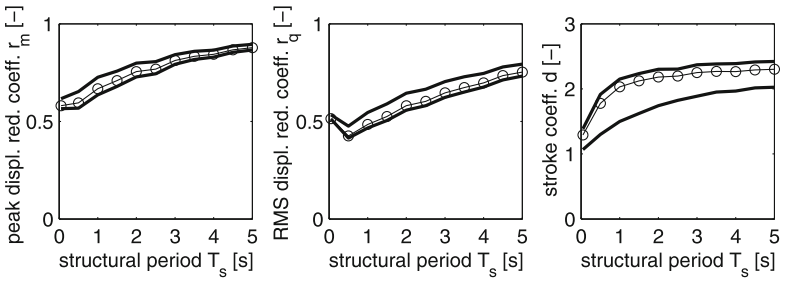

Fig. 3.11 *Left subplot*: bounds of set-valued peak displacement reduction coefficient R_{m} (*outer lines*), peak displacement reduction coefficient $r_{\mathrm{m},\bar{a}}$ (*central line*) for different values of T_{s}, and uncertain TMD frequency ω_{d}; *middle subplot*: bounds of set-valued RMS displacement reduction coefficient R_{q} (*outer lines*), RMS displacement reduction coefficient $r_{\mathrm{q},\bar{a}}$ (*central line*) for different values of T_{s}, and uncertain TMD frequency ω_{d}; *right subplot*: bounds of set-valued stroke coefficient D (*outer lines*), stroke coefficient $d_{\bar{a}}$ (*central line*) for different values of T_{s}, and uncertain TMD frequency ω_{d}

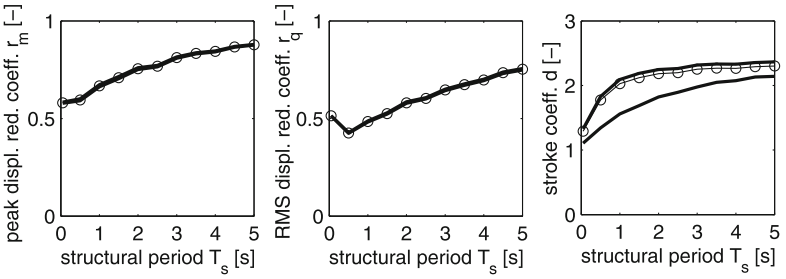

Fig. 3.12 *Left subplot*: bounds of set-valued peak displacement reduction coefficient R_{m} (*outer lines*), peak displacement reduction coefficient $r_{\mathrm{m},\bar{a}}$ (*central line*) for different values of T_{s}, and uncertain TMD damping ζ_{d}; *middle subplot*: bounds of set-valued RMS displacement reduction coefficient R_{q} (*outer lines*), RMS displacement reduction coefficient $r_{\mathrm{q},\bar{a}}$ (*central line*) for different values of T_{s}, and uncertain TMD damping ζ_{d}; *right subplot*: bounds of set-valued stroke coefficient D (*outer lines*), stroke coefficient $d_{\bar{a}}$ (*central line*) for different values of T_{s}, and uncertain TMD damping ζ_{d}

is coherent with the outcomes of [37, 38] based on real recorded ground motions. However, the stroke coefficient is influenced by ζ_{d} in a similar manner as by ω_{d}, i.e., the bounds of the set-valued stroke coefficient are only slightly tighter as in the right picture of Fig. 3.11.

In a further simulation, for both TMD parameters ω_{d} and ζ_{d} Tchebycheff random sets are used. Their approximations are combined to a two-dimensional random set by taking the cartesian product of each of the focal elements of the first with each of the focal elements of the second random set and multiplying the corresponding probability weights. This results in a finite random set consisting of 100 rectangular focal elements. In Fig. 3.13 the expectations of the reduction coefficients and the stroke coefficient are depicted. The plots of the reduction coefficients look very similar to the ones in Fig. 3.11, which emphasizes that the impact of TMD damping ζ_{d} on the reduction coefficient is small.

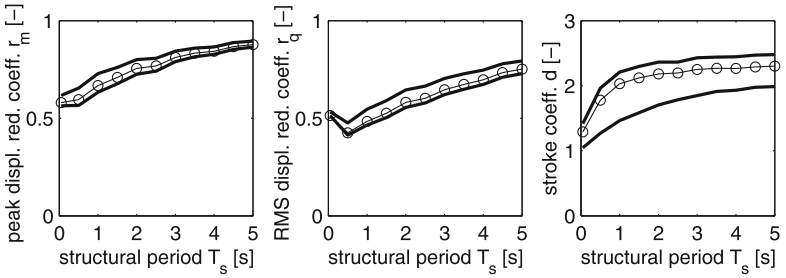

Fig. 3.13 *Left subplot*: bounds of set-valued peak displacement reduction coefficient R_{m} (*outer lines*), peak displacement reduction coefficient $r_{\mathrm{m},\overline{a}}$ (*central line*) for different values of T_{s}, and uncertain TMD parameters ω_{d}, ζ_{d}; *middle subplot*: bounds of set-valued RMS displacement reduction coefficient R_{q} (*outer lines*), RMS displacement reduction coefficient $r_{\mathrm{q},\overline{a}}$ (*central line*) for different values of T_{s}, and uncertain TMD parameters ω_{d}, ζ_{d}; *right subplot*: bounds of set-valued stroke coefficient D (*outer lines*), stroke coefficient $d_{\overline{a}}$ (*central line*) for different values of T_{s}, and uncertain TMD parameters ω_{d}, ζ_{d}

From all three figures one can see that the RMS displacement reduction coefficients are smaller than the peak displacement reduction coefficients. This is due to the fact that in the left pictures only the peak displacements of the trajectories are compared. These maximum displacements usually appear during the period of strong ground motion (where the intensity function equals 1). On the other hand, for the RMS displacement reduction all the displacements observed during the time interval are taken into account. Furthermore, one can observe that the bounds of the set-valued stroke coefficient are much wider than for the reduction coefficients, and that the stroke coefficient $d_{\overline{a}}$ induced by the optimal values of the TMD parameters are close to the upper bound of the set-valued stroke coefficient. These results lead to the well-known conclusion that the optimal TMD parameters from Eq. (3.3) lead to a large stroke, but by variation of the TMD parameters the stroke can be diminished considerably while the efficiency of the TMD is only deteriorating slightly, see, e.g., [37] .

Figure 3.14 shows the bounds of sample functions of the non-dimensional displacement Y of the load-bearing structure (bold lines) obtained by choosing two particular focal elements, a particular path of the ground motion process, and $T_{\mathrm{s}} = 1\,\mathrm{s}$. Thin lines represent the corresponding sample functions of the non-dimensional displacement $y_{\overline{a}}$ obtained for the nominal parameter values $\overline{a} = (\overline{\omega}_{\mathrm{d}}, \overline{\zeta}_{\mathrm{d}})$ and the non-dimensional structural displacement $\tilde{y}$ when no TMD is attached. In the left subplot of Fig. 3.15 the mean value functions of $|Y|$, $|y_{\overline{a}}|$ and $|\tilde{y}|$ for $T_{\mathrm{s}} = 1\,\mathrm{s}$ are plotted. One can see that during the phase of strong ground motion the displacements of the load-bearing system damped by the TMD are fluctuating around a constant value. Due to the increased damping by the TMD, these displacements decay much more quickly than the displacements of the TMD-free system after the end of the strong motion period. The right-hand subplot of Fig. 3.15 depicts for each time the probability that the non-dimensional

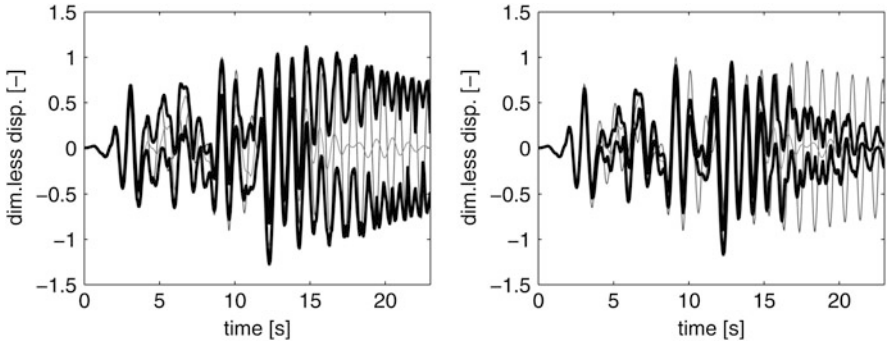

Fig. 3.14 Bounds of a sample function of the non-dimensional structural displacement Y (*bold lines*) and sample functions of $y_{\overline{a}}$ (*central thin line*) and $\tilde{y}$ (*outer thin line*) for $T_s = 1\,\mathrm{s}$ and two different focal elements for uncertain TMD parameters ω_d, ζ_d

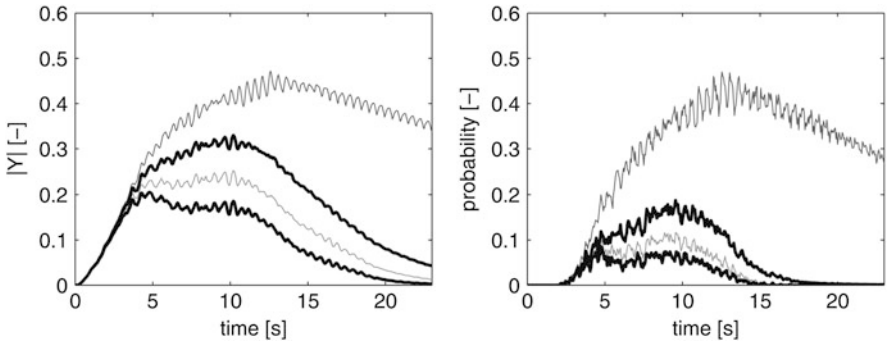

Fig. 3.15 *Left subplot*: mean value functions of the absolute values of the non-dimensional structural displacement $|Y|$ (*bold lines*), $|y_{\overline{a}}|$ (*central thin line*) and $|\tilde{y}|$ (*outer thin line*) for $T_s = 1\,\mathrm{s}$, and uncertain TMD parameters ω_d, ζ_d; *right subplot*: upper and lower probabilities of $[0.5, \infty)$ for $|Y|$ (*bold lines*), probabilities of $|y_{\overline{a}}| > 0.5$ (*central thin line*) and $|\tilde{y}| > 0.5$ (*outer thin line*), TMD parameters ω_d and ζ_d uncertain

displacement exceeds the value 0.5. For the set-valued process $|Y|$ this corresponds to the upper and lower probabilities of the interval $[0.5, \infty)$ (see Eq. (3.11)).

3.6.3 Set-Valued Soil Parameters

In this subsection, results of simulations are discussed when random sets are used for the soil parameters ω_g, ζ_g whereas the mass ratio, the structural damping, and the TMD parameters are fixed to their nominal values.

Figure 3.16 shows the expectations of the reduction coefficients and the stroke coefficient for soil damping $\zeta_g = 0.9$ and a Tchebycheff random set with nominal soil frequency $\overline{\omega}_g = 5\,\mathrm{rad/s}$. The coefficient of variation used for ω_g is 0.04.

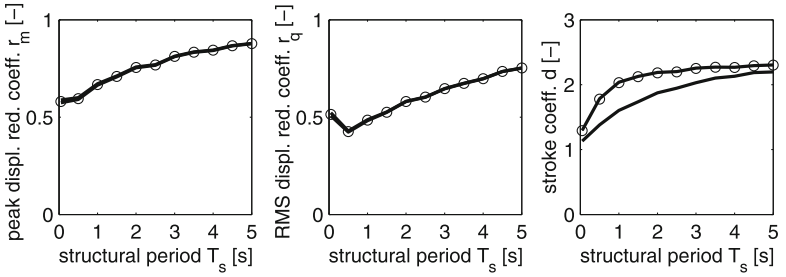

Fig. 3.16 *Left subplot*: bounds of set-valued peak displacement reduction coefficient R_{m} (*outer lines*), peak displacement reduction coefficient $r_{\mathrm{m},\bar{a}}$ (*central line*) for different values of T_{s}, and uncertain soil frequency ω_{g}; *middle subplot*: bounds of set-valued RMS displacement reduction coefficient R_{q} (*outer lines*), RMS displacement reduction coefficient $r_{\mathrm{q},\bar{a}}$ (*central line*) for different values of T_{s}, and uncertain soil frequency ω_{g}; *right subplot*: bounds of set-valued stroke coefficient D (*outer lines*), stroke coefficient $d_{\bar{a}}$ (*central line*) for different values of T_{s}, and uncertain soil frequency ω_{g}

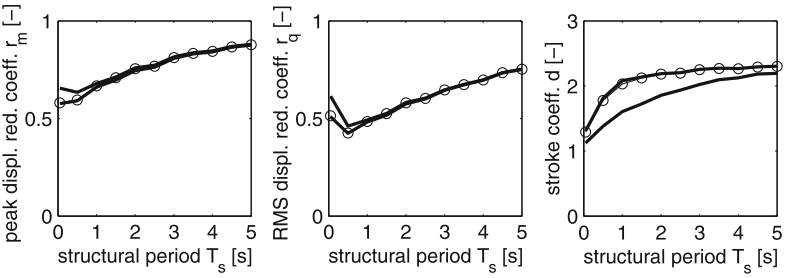

Fig. 3.17 *Left subplot*: bounds of set-valued peak displacement reduction coefficient R_{m} (*outer lines*), peak displacement reduction coefficient $r_{\mathrm{m},\bar{a}}$ (*central line*) for different values of T_{s}, and uncertain soil damping ζ_{g}; *middle subplot*: bounds of set-valued RMS displacement reduction coefficient R_{q} (*outer lines*), RMS displacement reduction coefficient $r_{\mathrm{q},\bar{a}}$ (*central line*) for different values of T_{s}, and uncertain soil damping ζ_{g}; *right subplot*: bounds of set-valued stroke coefficient D (*outer lines*), stroke coefficient $d_{\bar{a}}$ (*central line*) for different values of T_{s}, and uncertain soil damping ζ_{g}

Obviously, varying ω_{g} changes the reduction coefficients only slightly whereas the stroke coefficient is affected considerably. One can further consider the case where $\omega_{\mathrm{g}} = 5\,\mathrm{rad/s}$ and a random set is used for ζ_{g}. As before the nominal value of 0.9 is employed for soil damping ζ_{g}. Concerning the variability it is assumed that ζ_{g} can take values from 0.3 to 0.95; note that ζ_{g} is bounded by 1. This range does not lie symmetrically around the nominal value, and thus it is not appropriate to use a Tchebycheff random set. However, it seems reasonable to utilize a triangular random set instead as shown in Fig. 3.4, right subplot. The latter is approximated by the finite random set obtained by the choices $v_{\mathbb{A},j} = 0.01 + 0.11 \cdot (j-1)$, $j = 1, \ldots, 10$, with probability weights $p_1 = 0.01$, $p_j = 0.11$, $j = 2, \ldots, 10$. Figure 3.17 depicts the expectations of the resulting reduction coefficients and the

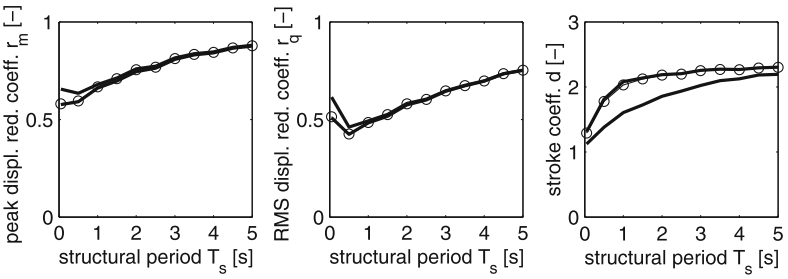

Fig. 3.18 *Left subplot*: bounds of set-valued peak displacement reduction coefficient R_{m} (*outer lines*), peak displacement reduction coefficient $r_{\mathrm{m},\bar{a}}$ (*central line*) for different values of T_{s}, and uncertain soil parameters ω_{g}, ζ_{g}; *middle subplot*: bounds of set-valued RMS displacement reduction coefficient R_{q} (*outer lines*), RMS displacement reduction coefficient $r_{\mathrm{q},\bar{a}}$ (*central line*) for different values of T_{s}, and uncertain soil parameters ω_{g}, ζ_{g}; *right subplot*: bounds of set-valued stroke coefficient D (*outer lines*), stroke coefficient $d_{\bar{a}}$ (*central line*) for different values of T_{s}, and uncertain soil parameters ω_{g}, ζ_{g}

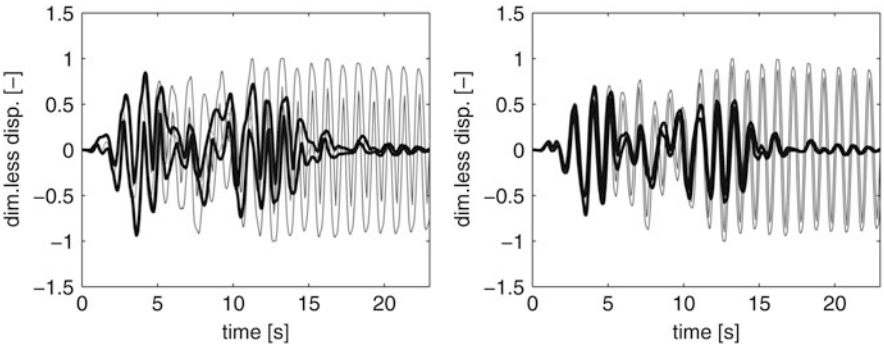

Fig. 3.19 Bounds of sample functions of the non-dimensional structural displacement Y (*bold lines*), sample functions of $y_{\bar{a}}$ (*central thin line*) and bounds of sample functions of $\tilde{Y}$ (*outer thin lines*) for $T_{\mathrm{s}} = 1$ s and two different focal elements for uncertain soil parameters ω_{g}, ζ_{g}

stroke coefficient. Obviously, for the reduction coefficients significant deviations from the nominal values can only be recognized for structural periods T_{s} up to 1 s. For larger values of T_{s} the bounds of the set-valued reduction coefficients more or less coincide with the reductions computed with the nominal values. Similar to Fig. 3.16 the stroke coefficient varies considerably. Very similar outcomes are found when using random sets for both parameters ω_{g} and ζ_{g} (see Fig. 3.18). Figure 3.19 shows sample functions, and in Fig. 3.20 mean value functions and exceedance probabilities are plotted.

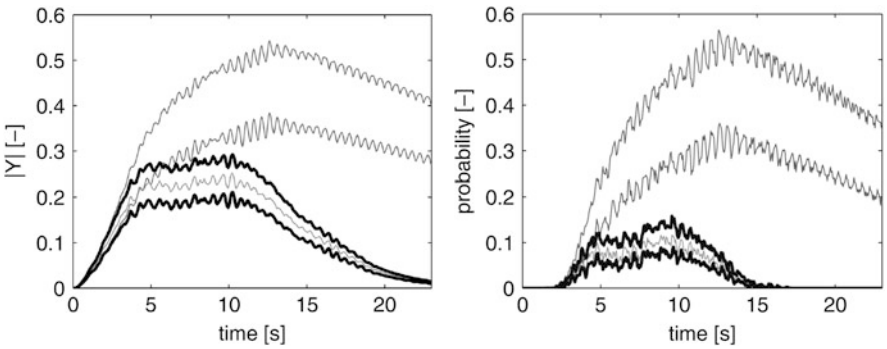

Fig. 3.20 *Left subplot*: mean value functions of the absolute values of non-dimensional structural displacement $|Y|$ (*bold lines*), $|y_{\overline{a}}|$ (*central thin line*) and $|\widetilde{Y}|$ (*outer thin lines*) for $T_s = 1$ s, soil parameters ω_g and ζ_g uncertain; *right subplot*: upper and lower probabilities of $[0.5, \infty)$ for $|Y|$ (*bold lines*) and $|\widetilde{Y}|$ (*outer thin lines*), probabilities of $|y_{\overline{a}}| > 0.5$ (*central thin line*), soil parameters ω_g and ζ_g uncertain

3.7 Conclusion

In this paper a framework to assess the seismic performance of Tuned Mass Dampers (TMDs) in presence of parameter uncertainty has been presented. A stochastic process, based on the Kanai–Tajimi power spectral density function, models earthquake excitation. This constitutes a more realistic excitation model than white noise used in an earlier study [29]. Random sets have been used to describe the uncertainty of the ground parameters and the TMD parameters, which can (in practice) not be tuned optimally. The benefit is an adequate assessment of response reduction coefficients of the main system and the stroke coefficient of the TMD system. The interval-valued description of the behavior of the TMD system is more informative and reliable than a purely stochastic description with single-valued outputs.

Based on this methodology a parametric study has been conducted to quantify the efficiency of a TMD to reduce the seismic response of a vibration-prone structure that can be modeled sufficiently accurately as a single degree-of-freedom oscillator. The results derived are coherent with the outcomes of a similar parametric study [37] that is, however, based on a set of recorded earthquake ground motions. The considered response quantities are both qualitatively and quantitatively comparable, and thus the analytical expression for seismic TMD design presented in [37] is confirmed. Beneficially, the utilized stochastic ground motion model allows one to study the effect of a targeted variation of specific ground motion parameters on the TMD performance, as it has been conducted here.

References

1. Adam, C., Furtmüller, T.: Seismic performance of Tuned Mass Dampers. In: Irschik, H., Krommer, M., Watanabe, K. (eds.) Mechanics and Model Based Control of Smart Materials and Structures, pp. 11–18. Springer, Wien (2010)
2. Arnold, L.: Stochastic Differential Equations: Theory and Applications. Wiley, New York (1974)
3. Ayorinide, E.O., Warburton, G.B.: Minimizing structural vibrations with absorbers. Earthquake Eng. Struct. Dyn. **8**, 219–236 (1980)
4. Bucher, C.: Computational Analysis of Randomness in Structural Mechanics. CRC Press/Balkema, Leiden (2009)
5. Casciati, F., Giuliano, F.: Performance of multi-TMD in the towers of suspension bridges. J. Vibr. Contr. **15**, 821–847 (2009)
6. Clough, R.W., Penzien, J.: Dynamics of Structures. Mc Graw-Hill, Auckland (1975)
7. Dempster, A.P.: Upper and lower probabilities induced by a multivalued mapping. Ann. Math. Stat. **38**, 325–339 (1967)
8. Den Hartog, J.P.: Mechanical Vibrations. 4th edn. McGraw-Hill, New York (1956)
9. Building Code EN 1998-1: Eurocode 8: Design of structures for earthquake resistance – Part 1: General rules, seismic actions and rules for buildings, 2005.
10. Fetz, T., Oberguggenberger, M.: Propagation of uncertainty through multivariate functions in the framework of sets of probability measures. Reliab. Eng. Syst. Safety **85**, 73–87 (2004)
11. Goodman, I.R., Nguyen, H.T.: Fuzziness and randomness. In: Bertoluzza, C., Gil, M.Á., Ralescu, D.A. (eds.) Statistical Modeling Analysis and Management of Fuzzy Data. Physica, Heidelberg (2002)
12. Hall, J., Rubio, E., Anderson, M.: Random sets of probability measures in slope hydrology and stability analysis. Zeitschrift für Angewandte Mathematik und Mechanik **84**, 710–720 (2004)
13. Hoang, N., Fujino, Y., Warnitchai, P.: Optimal Tuned Mass Damper for seismic applications and practical design formulas. Eng. Struct. **30**, 707–715 (2008)
14. Jensen, H., Setareh, M., Peek, R.: TMDs for vibration control of systems with uncertain properties. J. Struct. Eng. **118**, 3285–3296 (1992)
15. Kanai, K.: Semi-empirical formula for the seismic characteristics of the ground motion. Bull. Earthquake Res. Inst. Univ. Tokyo **35**, 309–325 (1957)
16. Kloeden, P.E., Platen, E.: Numerical Solution of Stochastic Differential Equations. Springer, Berlin (1992)
17. Leung, A.Y.T., Zhang, H., Chen, C.C., Lee, Y.Y.: Particle swarm optimization of TMD by non-stationary base excitation during earthquake. Earthquake Eng. Struct. Dyn. **37**, 1223–1246 (2008)
18. Meinhardt, C.: Experimental damping assessments of tall buildings to verify the effectivity of damping devices for high rise structures. In: Proceedings of the International Conference on Highrise Towers and Tall Buildings 2010, Munich, Germany, CD-ROM paper, 14–16 April 2010
19. Molchanov, I.: Theory of Random Sets. Springer, Berlin (2005)
20. Nguyen, H.T.: An Introduction to Random Sets. Chapman and Hall/CRC Press, Boca Raton (2006)
21. Oberguggenberger, M.: The mathematics of uncertainty: models, methods and interpretations. In: Fellin, W., Lessmann, H., Oberguggenberger, M., Vieider, R. (eds.) Analyzing Uncertainty in Civil Engineering. Springer, Berlin (2005)
22. Øksendal, B.: Stochastic Differential Equations. An Introduction with Applications. Springer, Berlin (1998)
23. Peil, U., Clobes, M.: Erdbebenbeanspruchung abgespannter Maste. Bauingenieur **87**, 124–129 (2012)
24. Rackwitz, R.: Einwirkungen auf Bauwerke. In: Mehlhorn, G. (ed.) Der Ingenieurbau: Grundwissen, Bd. 8, Tragwerkszuverlässigkeit/Einwirkungen, pp. 73–416. Ernst & Sohn, Berlin (1997)

25. Rofooei, F.R., Mobarake, A., Ahmadi, G.: Generation of artificial earthquake records with a nonstationary Kanai-Tajimi model. Eng. Struct. **23**, 827–837 (2001)
26. Sadek, F., Mohraz, B., Taylor, A.W., Chung, R.M.: A method for estimating the parameters of Tuned Mass Dampers for seismic applications. Earthquake Eng. Struct. Dyn. **26**, 617–635 (1997)
27. Schmelzer, B.: On solutions of stochastic differential equations with parameters modelled by random sets. Int. J. Approx. Reason. **51**, 367–376 (2010)
28. Schmelzer, B., Adam, C., Oberguggenberger, M.: Seismic performance of Tuned Mass Dampers with uncertain parameters. In: Eberhardsteiner, J., Böhm, H.J., Rammerstorfer, F.G. (eds.) Proceedings of the 6th European Congress on Computational Methods in Applied Sciences and Engineering (ECCOMAS 2012), p. 20, Vienna, Austria, CD-ROM paper, 10–14 September 2012
29. Schmelzer, B., Oberguggenberger, M., Adam, C.: Efficiency of tuned mass dampers with uncertain parameters on the performance of structures under stochastic excitation. Proceedings of the Institution of Mechanical Engineers. Part O J. Risk Reliab. **224**, 297–308 (2010)
30. Shafer, G.: A Mathematical Theory of Evidence. Princeton University Press, Princeton (1976)
31. Soong, T.T.: Active Structural Control: The Theory and Practice. Longman Scientific and Technical Series, New York (1990)
32. Soong, T.T., Dargush, G.F.: Passive Energy Dissipation Systems in Structural Engineering. Wiley, Chichester (1997)
33. Soong, T.T., Grigoriu, M.: Random Vibration of Mechanical and Structural Systems. Prentice-Hall, Englewood Cliffs (1993)
34. Tajimi, H.: A statistical method of determining the maximum response of a building structure during an earthquake. In: Proceedings of the 2nd Conference on Earthquake Engineering, vol. 2, pp. 781–798. Science Council of Japan, Tokyo (1960)
35. Tonon, F., Bernardini, A., Mammino, A.: Determination of parameters range in rock engineering by means of random set theory. Reliab. Eng. Syst. Saf. **70**, 241–261 (2000)
36. Tonon, F., Bernardini, A., Mammino, A.: Reliability analysis of rock mass response by means of random set theory. Reliab. Eng. Syst. Saf. **70**, 263–282 (2000)
37. Tributsch, A., Adam, C.: Evaluation and analytical approximation of Tuned Mass Damper performance in an earthquake environment. Smart Struct. Syst. **10**, 155–179 (2012)
38. Tributsch, A., Adam, C., Furtmüller, T.: Mitigation of earthquake induced vibrations by Tuned Mass Dampers. In: De Roeck, G., Degrande, G., Lombaert, G., Müller, G. (eds.) Structural Dynamics - EURODYN2011, Proceedings of 8th European Conference on Structural Dynamics, pp. 1742–1749, Leuven, Belgium, CD-ROM paper, 4–6 July 2011
39. Wang, J.-F., Lin, C.-C., Lian, C.-H.: Two-stage optimum design of tuned mass dampers with consideration of stroke. Struct. Control Health Monit. **16**, 55–72 (2009)
40. Warburton, G.B.: Optimum absorber parameters for various combinations of response and excitation parameters. Earthquake Eng. Struct. Dyn. **10**, 381–401 (1982)